Published in final edited form as:

Methods Enzymol. 2016 ; 581: 285–315. doi:10.1016/bs.mie.2016.08.012.

Single-Molecule FRET to Measure Conformational Dynamics of DNA Mismatch Repair Proteins

J.W. Gauer[*], **S. LeBlanc**[*], **P. Hao**[†], **R. Qiu**[†], **B.C. Case**[‡], **M. Sakato**[‡], **M.M. Hingorani**[‡], **D.A. Erie**[*,1], and **K.R. Weninger**[†,1]

[*]University of North Carolina at Chapel Hill, Chapel Hill, NC, United States

[†]North Carolina State University, Raleigh, NC, United States

[‡]Wesleyan University, Middletown, CT, United States

Abstract

Single-molecule FRET measurements have a unique sensitivity to protein conformational dynamics. The FRET signals can either be interpreted quantitatively to provide estimates of absolute distance in a molecule configuration or can be qualitatively interpreted as distinct states, from which quantitative kinetic schemes for conformational transitions can be deduced. Here we describe methods utilizing single-molecule FRET to reveal the conformational dynamics of the proteins responsible for DNA mismatch repair. Experimental details about the proteins, DNA substrates, fluorescent labeling, and data analysis are included. The complementarity of single molecule and ensemble kinetic methods is discussed as well.

1. INTRODUCTION

1.1 Single-Molecule FRET to Measure Protein Conformation

Understanding how changes in protein conformation are linked to function is a key step in modeling molecular mechanisms for many enzymes. Among experimental methods that measure protein conformational changes, fluorescence resonance energy transfer (Förster resonance energy transfer, FRET) has proven to be of great use for sensitive detection of protein dynamics in physiologically relevant settings. FRET measurements are made by engineering macromolecules with two fluorophores attached at defined locations and measuring spectrally resolved fluorescence emission from these probes. Distance-dependent interaction between these fluorophores alters the overall emission spectrum, allowing the changes in signal to be interpreted as changes in molecular conformation. With proper corrections for systematic effects, these signals can be quantitatively related to nanometer dimensions, leading to the description of FRET as a “spectroscopic ruler” (Stryer & Haugland, 1967).

The power of FRET measurements to reveal dynamic protein conformational changes took a tremendous leap forward two decades ago when signals were successfully detected from a single molecule; this methodology is now called single-molecule FRET (smFRET) (Ha et

[1]Corresponding authors: derie@email.unc.edu; krwening@ncsu.edu.

al., 1996). Measuring FRET signals from single molecules avoids the averaging that dominates ensemble biochemical approaches. Single-molecule studies provide access to heterogeneous behaviors and the ability to monitor the dynamics of unsynchronizable populations of macromolecules, making it an ideal tool for investigating the role of conformational dynamics in enzyme function. Below, we describe single-molecule FRET assays that we have developed to study conformational dynamics of DNA mismatch repair (MMR) proteins.

1.2 Overview of Our DNA MMR Protein Experiments

Living organisms have a widely conserved system of proteins that locate and respond to DNA base–base mismatch and insertion errors made during replication, as well as damaged bases in DNA. The system, known as MMR, either repairs mismatches or leads to the activation of checkpoints that promote cell-cycle arrest or apoptosis in the case of damage (Bignami, Casorelli, & Karran, 2003; Fedier & Fink, 2004; Karran, Offman, & Bignami, 2003). MMR proteins play a fundamental role in genome stability and cellular homeostasis (Modrich & Lahue, 1996), and mutations in these proteins are associated with carcinogenesis (Heinen, 2016; Peltomaki, 2016).

MMR proteins MutS and MutL are responsible for detecting DNA mismatches and initiating the repair process. Both MutS and MutL homologues have DNA binding and ATPase activities that are essential for MMR in vivo (Iyer, Pluciennik, Burdett, & Modrich, 2006; Kunkel & Erie, 2005). Both proteins are homodimers in prokaryotes and heterodimers in eukaryotes. Here, our main goal is to describe smFRET methodology we have applied to our studies of the homodimeric MutS and MutL proteins from *Thermus aquaticus* (*Taq*). The mechanism of the *Taq* MMR system appears similar to that in most other species (with the notable exception of *Escherichia coli*), and therefore, we will simply call the proteins MutS and MutL in the following text.

The current consensus about key events occurring in MMR initiation is that MutS slides along double-stranded DNA searching for the rare mismatched or damaged base. It binds to mismatches (Fig. 1), at which point ATP induces conformational changes in MutS that can result in a mobile clamp state that moves along the DNA. This ATP and mismatch activated state of MutS has enhanced interactions with MutL, resulting in MutL stabilizing MutS at the mismatch (Groothuizen et al., 2015; Qiu et al., 2015; Schofield, Nayak, Scott, Du, & Hsieh, 2001). Interactions between the MutS-activated MutL complex and the replication processivity clamp (β-clamp in prokaryotes and PCNA in eukaryotes) can activate MutL to incise the newly replicated strand up to hundreds of bases from the mismatch both distally (preferential) and proximally to the mismatch (Kadyrov, Dzantiev, Constantin, & Modrich, 2006; Kadyrov et al., 2007; Pluciennik, Burdett, Lukianova, O'Donnell, & Modrich, 2009). MutS then stimulates exonucleases to begin degrading the newly synthesized strand from the MutL-created nick (or possibly from preexisting nicks/gaps in the strand). The resulting gap that typically extends past the mismatch is then resynthesized and remaining nicks are ligated to complete repair (Genschel & Modrich, 2003, 2009; Iyer et al., 2006; Kunkel & Erie, 2005, 2015; Liberti, Larrea, & Kunkel, 2013; Morita et al., 2010; Nick McElhinny, Kissling, & Kunkel, 2010; Pavlov, Mian, & Kunkel, 2003).

Initiation of MMR involves an ordered choreography of interactions between DNA, MutS, and MutL coupled with the ATPase reaction. Many studies using X-ray crystallography (Lamers et al., 2000; Natrajan et al., 2003; Obmolova, Ban, Hsieh, & Yang, 2000; Warren et al., 2007), AFM (Wang et al., 2003), and ensemble biochemistry (Fishel, 2015; Iyer et al., 2006; Kunkel & Erie, 2005) have suggested that these interactions involve substantial conformational changes in both the DNA and the proteins, but the dynamics of these events have been difficult to resolve. Our studies of these interactions at the single-molecule level have allowed us to characterize in detail large DNA bending transitions, conformational changes within the MutS mismatch binding domains that are dependent on ATP and the mismatch, as well as MutL interactions that alter these conformational trajectories. These observations, coupled with data from ensemble transient kinetics, have yielded a highly detailed view of the molecular mechanisms used by this enzyme system to identify, verify, and begin repairing DNA mismatch errors. The goal here is to describe these experimental smFRET approaches. The application of a broader range of single-molecule methods to study DNA MMR is reviewed elsewhere (Erie & Weninger, 2014). The studies described here are widely applicable to other biological systems in which the proteins can be purified and fluorescently tagged.

2. METHODS OF ACQUIRING FRET SIGNALS FROM *T. aquaticus* DNA MMR PROTEINS

For a FRET experiment, two fluorophores with distinct spectral characteristics must be attached to the molecule of interest (Fig. 2). The fluorophore with the shorter wavelength emission (called donor) is excited with an external light source. If the longer wavelength fluorophore (called acceptor) is further from the donor than the effective FRET range, then no FRET occurs and only donor emission is observed. FRET processes can excite the acceptor when it is within about 7–8 nm of the donor, which then decreases the donor emission and increases the acceptor emission. The FRET efficiency is defined as $E = I_A/(I_D + I_A)$, where I_D and I_A are the donor and acceptor emission intensities. FRET efficiency is a useful parameter because it is related to the distance d between the fluorophores by $E = 1/(1+(d/R_0)^6)$, where R_0 (the Förster radius) sets the scale of the FRET effect. R_0 is a function of the properties of the fluorophores and typically ranges about 4–6 nm. The dependence on the sixth power of distance makes FRET very sensitive in the R_0 range (Fig. 2B).

Our experiments utilize total internal reflection fluorescence (TIRF) microscopy to observe MMR proteins interacting with DNA tethered to the surface of a flow cell. Methodological details of these experiments are described below.

2.1 Proteins

We work with MMR proteins from the thermophile *Taq*, which have proved to be stable in vitro and amenable to structure–function analysis by a wide variety of techniques, including smFRET. The *Taq* MutS monomer is 811 amino acids with a molecular weight ~90 kDa, and the *Taq* MutL monomer is 532 amino acids with a molecular weight ~59 kDa. MutS has one native cysteine that is mutated to alanine and, for the studies described below, methionine 88

is replaced with cysteine for labeling the DNA binding domain. Neither mutation alters DNA binding or ATPase rates (Sharma, Doucette, Biro, & Hingorani, 2013). *Taq* MutL has three native cysteines and none labeled when treated with maleimide dye; consequently, introduction of a surface-exposed cysteine is sufficient for site-specific labeling of MutL. Mutations were performed in the overexpression plasmid using the Quickchange II XL kit (Agilent). Note that *Taq* genes are GC rich, which makes PCR and sequencing difficult and less reliable. Multiple reactions are necessary to confirm successful manipulations.

2.1.1 Preparation of *Taq* MutS

Expression: Express MutS in pET3a plasmid in BL21-DE3 *E. coli* in LB media including 50 μg/mL Ampicillin at 37°C until OD 0.5 and then add IPTG to 0.1 m*M*. After expression for 3 h, collect cells by centrifugation.

Purification: Resuspend cells in lysis buffer (20 m*M* HEPES–NaOH pH 7.8, 100 m*M* NaCl, 1 m*M* EDTA, 0.1 m*M* DTT, 1 m*M* PMSF, protease inhibitor cocktail), sonicate to lyse, centrifuge at 40,000 rpm for 30 min at 4°C (Beckman MLA-80 Rotor), collect supernatant and heat to 65°C for 30 min (*Taq* MutS is thermostable), cool to room temperature, centrifuge at 8000 rpm for 20 min at 4°C (Eppendorf F34-6-38 Rotor), collect supernatant and add ammonium sulfate (36.6 g/100 mL supernatant, final ~60% saturation), agitate 4°C for 15 min, centrifuge 10,000 rpm for 20 min 4°C (Eppendorf F34-6-38 Rotor), resuspend pellet in Tris-50 buffer (20 m*M* Tris–HCl pH 7.8, 50 m*M* NaCl, 0.5 m*M* DTT), and dialyze against the same buffer with several changes. Load sample onto Hi-TRAP Sepharose Q column, wash with Tris-50 buffer, and then elute with an NaCl gradient to 1 *M* (MutS elutes around 150–300 m*M* NaCl). Dialyze the protein against Tris-50 buffer with several changes. Load onto a MonoQ column. Wash with Tris-50 buffer and then elute with an NaCl gradient to 1 *M* (MutS elutes around 200–300 m*M* NaCl). Dialyze in *Taq* storage buffer (20 m*M* HEPES–NaOH pH 7.8, 1 m*M* EDTA, 10% glycerol, 150 m*M* NaCl, 0.1 m*M* DTT) and snap freeze for storage at −80°C.

Labeling: To label MutS with maleimide fluorophores, exchange storage buffer with label buffer (20 m*M* phosphate, pH 7.2, 150 m*M* NaCl) using a Sephadex G-25 column (Nap5, PD10, GE Biosciences). Add TCEP at 10 × concentration over free cysteines for 5 min at room temperature. Then add maleimide reactive dye at 10 × concentration over free cysteines. Incubate 1 h to overnight. Remove unreacted dye using the Sephadex G-25 or G-50 desalting column or by dialysis against Tris-50 buffer.

2.1.2 Preparation of *Taq* MutL

Expression: Express MutL from pET17b plasmid in BL21-DE3 *E. coli* in LB media including 50 μg/mL Ampicillin at 37°C until OD 0.5, and then induce the expression with 0.5 m*M* IPTG. After expression for 3–4 h, collect cells by centrifugation.

Purification: Suspend cells in ice-cold lysis buffer (20 m*M* Tris–HCl pH 7.5, 0.5 *M* NaCl, 5 m*M* imidazole) augmented with protease inhibitors and PMSF. Sonicate on ice until cells are disrupted. Centrifuge at 35,000 rpm for 30 min (Beckman MLA-80 Rotor). Add supernatant to Ni-NTA agarose resin equilibrated in lysis buffer. Incubate 1 h at 4°C. Wash the Ni-NTA

column in lysis buffer+60 m*M* imidazole. Elute in lysis buffer+300 m*M* imidazole (dimeric MutL elutes at ~300 m*M* imidazole). Dialyze against lysis buffer without imidazole overnight. Freezing before labeling with liquid nitrogen is acceptable.

Labeling: To label MutL with maleimide fluorophores, exchange buffer with label buffer (20 m*M* phosphate pH 7.2, 500 m*M* NaCl) using a P6 column (Bio-Rad Bio-Gel P-6DG). Note that *Taq* MutL binds nonspecifically to Sephadex G-25 matrix, but flows through P6 gel. Add TCEP at 10 × concentration over free cysteines for 5 min at room temperature. Then add maleimide reactive dye at 10 × concentration over free cysteines. Incubate 1 h to overnight. Remove unreacted dye from MutL using the P6 desalting column in labeling buffer. Use immediately, freezing the labeled protein leads to aggregation for MutL.

2.2 Preparation of DNA Substrates

smFRET experiments have been performed with either 50 nucleotide (nt) or 550 nt dsDNA substrates. Both lengths of DNA include a biotin on one end to allow immobilization on a streptavidin-coated surface. The 550 nt dsDNA has a digoxin on the other end to allow end blocking by treatment with digoxigenin (dig) antibody. The 50 nt dsDNA substrate can be constructed from oligos ordered from commercial vendors. A 50 nt oligo with a 5′-biotin and a 3′-donor fluorophore is annealed to a 19 nt oligo with sequence complementary to the 3′-end of the 50 nt oligo (except a mismatched base at position 9). This 19 nt oligo has an acceptor fluorophore on its 3′-end that makes a FRET pair 19 bases apart with a mismatched base centered in between. A 31 nt oligo is annealed to fill the remaining ssDNA gap.

A more complex process is required to construct the 550 nt dsDNA substrate. PCR of a pUC-VSR plasmid template using oligos containing 5′-biotin and dig modifications is used to amplify a 550 nt section of the plasmid and introduce the biotin/dig moieties. A nicking endonuclease (Nt.BbvCI) is used to remove a central segment of one strand. Then an oligo is annealed to fill that gap. The oligo may include a mismatched base and fluorophores if desired. Ligase is used to seal the remaining nicks. A detailed protocol is given below:

Part 1—PCR and nicking

1. PCR
    a. Prepare PCR reactions: 5 μL of 10 × polymerase buffer, 50 pmol F1-biotin primer, 50 pmol R2-primer*, 50 ng pUC-VSR plasmid, water to 49 μL, and 1 μL *Taq* polymerase (Invitrogen AccuPrime *Taq* DNA Polymerase) (*use different end-modified primers for different types of end-modified DNA; our studies include R2 (Normal) primer, LacO primer, and Dig primer).
    b. Run PCR: 95°C for 1 min; [95°C for 1 min—55°C for 33 s—69°C for 50 s]$_{\text{repeat 32×}}$; 69°C for 5 min, 55°C for 5 min.
    c. Purify PCR product with PCR purification kit. Elute in 40 μL kit elution buffer. This is homo-duplex DNA.

2. Nicking
    a. Prepare nicking reaction with 5 μL 10 × NEB buffer 4, 1 μg PCR product DNA, 45 μL water, 5 μL Nt.BbvCI (NEB, Cat# R0632S).
    b. Incubate 37°C for 16 h.

Part 2—Gapping, phosphorylation, annealing, and ligation

1. Gapping:
    a. Add 250 μL (5 × volume) of Buffer PBI (Qiagen) to each nicked sample
    b. Incubate samples at 80°C for 20 min (heat inactivates any remaining Nt.BbvCI and also melts short nicked pieces away from 550 mer)
    c. Immediately spin each reaction through a QIAquick spin column
    d. Transfer to a new collection tube
    e. Add 750 μL of buffer PE and spin column (containing ethanol)
    f. Repeat spin in new collection tube to remove residual ethanol
    g. Transfer to a new collection tube (with cap)
    h. Add 30 μL of Buffer EB; allow to sit 1 min; spin to elute DNA
2. Phosphorylation: (If your oligo is commercially phosphorylated, skip this step. The yield of fully ligated product will be reduced if the oligo is not ordered phosphorylated.)
    a. Prepare your phosphorylation reactions with 20 pmol DNA, 2 μL 10 × kit reaction buffer, 0.2 μL ATP (100 μ*M* stock), 19 μL water, 1 μL PNK (T4 Polynucleotide Kinase, Fermentas, Cat# EK0031)
        1. Incubate 37°C for 1 h and then 70°C for 5 min (denature enzyme). There is no need for purification at this stage as it will result in significant loss of DNA
3. Annealing
    a. Prepare annealing reactions. Mix gapped DNA with ~1.5 × mismatch-containing oligo. Note: excess oligo will result in multiple dyes on a single DNA molecule
    b. Anneal at 70°C for 5 min and then ramp down temperature from 70°C to 16°C at 1°C per min (or let it cool down naturally to room temperature in heat block)
4. Purify the annealed product using a PCR purification kit to remove extra oligo in the reaction. Elute in 45 μL elution buffer
5. Ligation

a. Add 5 μL of *E. coli* DNA ligase buffer and 1.5 μL of *E. coli* DNA ligase to each reaction

b. Incubate at 16°C for 20 h

c. PCR purify the first ligation product (elute in 45 μL of elution buffer) and set up the second ligation reaction

d. Repeat three times

e. When the third ligation reaction is done, purify the final 550 nt DNA using a PCR purification kit

2.3 Considerations Related to Fluorescent Labeling

Several fluorescent tags are commercially available for labeling oligonucleotides (e.g., TAMRA, the Cy dyes, Alexa dyes). When choosing which specific fluorophores to use, it is important to select dyes with high extinction coefficients and quantum yields so that they can be easily detected at the single-molecule level. Also, the dyes' excitation and emission spectra should be compatible with the optical setup such that independent excitation and emission detection is possible for each dye. Donor–acceptor dye pairs commonly used in our smFRET experiments include Alexa 555-Alexa 647, Alexa 555-Cy5, TAMRA-Cy5, and Cy3-Cy5.

There are several unknown parameters that can complicate dye selection. Notably, the structures of several commercial fluorophores are proprietary; thus, any perturbations they may introduce into the DNA remain unknowable. Also, fluorophores that serve as effective reporters in bulk experiments may be prone to blinking or bleaching in single-molecule experiments, making them poor choices for conformational dynamics studies using smFRET. Finally, some dyes are prone to interactions with the DNA (e.g., stacking with the bases), which may change their fluorescence properties in ways that do not depend on DNA or MMR protein conformational changes.

Several chemical strategies exist to link fluorophores to DNA. Labeling the 5′- or 3′-ends of the DNA is one option; however, being limited to only the ends of the DNA may be problematic. While internally labeling DNA oligonucleotides allows flexibility in choosing labeling positions, there are fewer commercially available options for fluorophores. Two major types of internal labels are: (1) dyes attached covalently to thymine bases via a flexible linker extending from the major groove in the DNA, and (2) dyes (e.g., the Cy dyes) that can be incorporated directly into the DNA backbone. Note that these fluorophores are rigidly locked into a specific orientation relative to the DNA backbone as they are covalently attached at both ends, whereas fluorophores on a flexible linker have more conformational freedom. The Förster radius of a given FRET pair of fluorophores depends, in part, on the relative orientation of the transition dipoles of the two fluorophores (Lakowicz, 2006). Thus, limiting the conformational freedom of both fluorophores may lead to unpredictable changes in FRET due to changes in their relative orientations. In general, at least one freely rotating dye (i.e., those attached to flexible linkers) is recommended.

It is crucial that labeling positions are chosen beyond the binding footprint of the protein because the fluorescent properties are sensitive to changes in the local chemical environment. The crystal structure of *Taq* MutS shows protein–DNA contacts as far as 8 nucleotides from the mismatch (Fig. 1) (Obmolova et al., 2000); thus, fluorescent labels are placed outside this range.

2.4 TIRF Microscopy

Homemade flow cells constructed between a quartz microscope slide and a glass cover slip are built and samples are tethered to the surface through a biotin–streptavidin interaction. A quartz prism with index-matching oil at the contact with the quartz slide allows laser beam illumination to be directed to the sample above a microscope objective at an angle sufficiently steep that total internal reflection occurs at the quartz-buffer interface (Fig. 3A). The resultant evanescent field is used to excite fluorophores within a couple hundred nanometers of the interface. The illuminated area is imaged with a microscope objective onto an emCCD camera. A DualView image splitter (Photometrics) is used to split the image into two copies where each contains emission from either the donor or the acceptor spectral bands. These spectrally filtered images are relayed side by side onto the emCCD. Intensity vs time traces for spots identified to contain fluorophores are extracted from minute long movies. Detailed descriptions of flow-cell construction, sample immobilization, microscopy hardware, and extraction of single-molecule intensity vs time traces in donor and acceptor spectral emission bands are provided elsewhere (Choi, Weninger, & Bowen, 2012).

2.5 Overview of FRET Signals Reporting Different Conformational Aspects of DNA MMR Protein Complexes

We used smFRET to deduce conformations of several different aspects of the MutS:DNA complex (Fig. 4). Using a donor and acceptor attached to DNA (forming a FRET pair with the mismatched base halfway in between; Fig. 4A), MutS induced bending at the mismatched base can be measured (DeRocco, Anderson, Piehler, Erie, & Weninger, 2010; DeRocco, Sass, Qiu, Weninger, & Erie, 2014; Sass, Lanyi, Weninger, & Erie, 2010). When the DNA is straight, the fluorophores are further apart than when the DNA is kinked at the mismatch. We also labeled the DNA binding domain of dimeric MutS (domain I) with a mixture of donor and acceptor dyes (Fig. 4B). Single-molecule measurements allowed us to specifically select the fraction of dimers with one donor and one acceptor and measure FRET from this mixed-fluorophore population. smFRET experiments were designed to detect conformational transitions within the DNA binding domains of MutS in the absence or presence of DNA mismatches (Qiu et al., 2012). Finally, a third label combination, where a donor is on MutS and an acceptor is on DNA 9 nt away from a mismatched base (Fig. 4C), provided information on the position of MutS near a mismatch (Qiu et al., 2012, 2015). Labels in the N-terminal domain of dimeric MutL were also used to provide smFRET signals addressing the configuration of these domains as MutL interacts with MutS to initiate repair.

3. DATA ANALYSIS

3.1 Quantitative vs Qualitative Interpretation of FRET as Distance

Quantitative conversion of measured FRET ratios into the distance between the donor and acceptor fluorophores is possible. It is critical to address systematic issues related to the efficiency of the instrumentation for detection of fluorescence emission as well as the impact of the local molecular environment on mobility or quantum yields of the donor and the acceptor after they are attached to the DNA or protein molecules (McCann, Choi, Zheng, Weninger, & Bowen, 2010). smFRET is being developed as a quantitative tool for structural biology applications by making such systematic corrections to the FRET measurements (Brunger, Strop, Vrljic, Chu, & Weninger, 2011; Choi et al., 2010). In contrast, for our DNA MMR studies, we have not interpreted FRET as indicating a quantitative distance, but rather have focused on analysis of the kinetics of transitions among distinct states (Fig. 3B).

3.2 Edge Detection in Time Traces for Kinetics

Given proper surface coverage by a sample of labeled oligonucleotide and protein, a single movie collected as described above may contain fluorescence information for over 100 DNA molecules. While already a large amount of information, the amount of data to analyze multiplies with varying experimental conditions and replicate experiments, thus an automated computational analysis approach vital. Automated analyses, however, require verification to identify unexpected patterns and check for systematic errors. Below, a computational analysis pipeline is presented that systematically applies an analysis routine and outputs the results for a user interface.

3.2.1 Extracting the Fluorescence Time Traces of Individual DNA Molecules—

Typical experiments produce movies made up of a series of approximately 1000 frames acquired at typically 10 Hz. As mentioned above, donor emission and acceptor emission from an area being imaged are recorded on side-by-side halves of the camera. By initially exciting only the acceptor dye, local maxima on the acceptor half of the image can be identified. These same locations mapped to the other half of the frame should locate the emissions from the donor dye. To determine the relative offset between the two halves of the image, broadband emission fluorescent beads fixed on a slide surface that appear in both halves of the image are imaged in separate calibration runs. These calibration images allow an experimentally determined offset to be determined, which is then applied to the experimental movies.

For each DNA molecule, the sum of the fluorescence intensities of a 3 × 3 pixel square centered on the local maxima pixel coordinates for the donor and acceptor dyes are determined. The local background intensity is subtracted, and those foci below a user set minimum threshold intensity are discarded. Foci too close to the camera edges or another focus are also discarded. For those foci that remain, the intensity is determined for each movie frame for both the donor and acceptor as the sum of the 4 highest pixels in the 3 × 3 square, ultimately resulting in a “time trace” of the donor and acceptor fluorescence emission intensities as a function of time (Fig. 3B, second row). Single-labeled donor or acceptor samples can be used to determine the fixed fraction of the emission that “leaks”

into the unintended channel. This fixed fraction that is a function of the fluorophore emission spectra and the optical filters can be subtracted from the acquired data.

3.2.2 Smoothing the Donor and Acceptor Time Traces Using the Chung–Kennedy Filter—Fluorescence intensity time traces have substantial noise deriving primarily from the shot noise of detection. Several methods exist to smooth noisy data, such as box-car averaging, but most of these smoothing methods do not preserve sharp edges. To overcome this limitation, Chung and Kennedy developed a nonlinear smoothing algorithm designed specifically to smooth data while preserving edges (Chung & Kennedy, 1991; Haran, 2004). This algorithm smoothes data containing transitions (Fig. 5A) by first determining the averages for windows of data of various sizes on either side of a given data point (dubbed the “forward” and “backward” average windows, Fig. 5B). To preserve edges, “forward” and “backward” averages that contain transitions are given less weight in the overall average. The statistical weights assigned to the “forward” and “backward” averages are determined as follows: The standard deviations for windows of data on either side of the data point being smoothed (referred to as the “forward” and “backward” predictor windows, Fig. 5C) are determined. The inverse of these standard deviations raised to a user-defined exponential term p is then used to calculate the statistical weights.

For example, consider a data point (at time i) with a transition occurring within the forward predictor window but not in the backward predictor window (Fig. 5A). The forward predictor window (Fig. 5C, green) would have a large standard deviation relative to the backward window (Fig. 5C, red). Thus, the averages from the forward average windows (Fig. 5B, green) would be assigned lower weight in the overall average, while the averages from backward average windows (Fig. 5B, red) would be assigned a larger statistical weight. This type of smoothing preserves transitions in the forward predictor window.

Importantly, in this approach the average windows and the predictor windows need not be the same size, nor is it necessary to use only one window size for each type of window. In fact, transitions that occur on different timescales can be preferentially preserved using windows of various sizes. Furthermore, the statistical weight term can be raised to the power of an empirically determined value (p) to exaggerate the different contributions of the forward and backward window averages. Thus, the input parameters of the average window size(s), predictor window size(s), and exponent term(s) can be defined by the user, and the optimal values in a given application can be empirically determined. Over filtering (i.e., introduction of false transitions) can be minimized by optimizing these input parameters.

When properly applied to the donor and acceptor time traces, the signal-to-noise ratio is significantly improved (Fig. 3B, third row), and transitions remain clear. Notably, in single-molecule FRET experiments, transitions in the donor and acceptor traces are expected to be anticorrelated (i.e., if the donor intensity increases, the acceptor intensity should simultaneously decrease, and vice versa). Because transitions in the donor and acceptor traces are expected to be simultaneous, the Chung–Kennedy smoothing algorithm can be improved by using the sum of the predictor window standard deviations for the both the donor and the acceptor to determine the statistical weights. As a result, simultaneous donor

and acceptor intensity transitions will be more strongly preserved compared to uncorrelated donor and acceptor changes in intensity (Chung & Kennedy, 1991; Haran, 2004).

3.2.3 Screening Time Traces for Data Quality—Time traces of insufficient quality should be discarded from analysis. There are several reasons a time trace or portions of a time trace may not be worth analyzing. For example, the detected fluorescence emission intensities may be too low to reliably detect changes in intensity, or they may be too high to represent emission from only one molecule. More commonly, either the donor or the acceptor fluorophore (or both) may permanently or temporarily lose its fluorescence properties (i.e., bleach or blink) during data acquisition.

To identify unanalyzable regions of time traces, the fluorescence intensity of each data point can first be checked against user-defined minimum and maximum thresholds. To assess for bleaches or blinks in the remaining data, the average and standard deviation of a moving seven-point window can be used to determine a 95% confidence interval for each data point. If this interval includes zero, the data point can be considered as part of a bleaching or blinking event and discarded from analysis. Time traces containing both analyzable and unanalyzable regions may contain useful information (e.g., prior to photobleaching). These regions can then be further analyzed to determine their quality.

3.2.4 Calculating FRET and Identifying Transitions in the FRET Time Traces— Analyzable regions of the remaining donor and acceptor time traces can then be used to calculate single-molecule FRET efficiency using the equation $E = I_A/(I_D + I_A)$, where I_D and I_A represent the background and leakage corrected, fluorescence emission intensities of the donor and acceptor fluorophores, respectively (DeRocco et al., 2014; Lakowicz, 2006; Qiu et al., 2012, 2015; Sass et al., 2010). The resulting FRET time trace (Fig. 3B, fourth row) contains several pieces of information: (1) the FRET efficiency at each point in time; (2) the dwell time of a given FRET state provides kinetic information, such as the characteristic lifetimes associated with each state; and (3) the transitions provide insight into the preferred pathways of conformational changes. To extract this information, it is crucial to identify the time point at which the FRET time trace undergoes a transition.

Several methods exist to detect transitions in data (Blanco & Walter, 2010; Greenfeld et al., 2015; McKinney, Joo, & Ha, 2006; Shuang et al., 2014; van de Meent, Bronson, Wiggins, & Gonzalez, 2014). Applying a transition detection method at different levels of stringency can minimize misidentification of transitions, as transitions that withstand more stringent thresholds are more likely to be “real.” Comparing the results of multiple methods can also help to overcome the limitations of using just one technique, as different detection methods will be better suited for detecting different types of changes (e.g., short- vs long-lived states) and will have different limitations. Edges detected by multiple methods at multiple stringency levels can then be assigned a higher confidence score. Presented here are two transition detection methods that can be independently applied at multiple thresholds to smFRET data.

Method 1: The Gaussian kernel method (Sass et al., 2010): Mathematically, transitions in continuous functions can be identified by finding inflection points (i.e., maxima and minima

in the first derivative of the time trace). Unfortunately, the FRET time traces are made up of discrete data points that have many apparent inflection points due to the significant noise in the signal. These issues can be circumvented by first convolving the FRET time traces with a Gaussian kernel of various widths and subsequently detecting inflection points in the convolved data. To ensure only “real” transitions are kept, a threshold can be incorporated. By changing the rigor of the threshold, the remaining “real” transitions can also be scored for confidence.

Method 2: The Chung-Kennedy method: The previously described smoothing algorithm developed by Chung and Kennedy uses increases in the predictor windows’ standard deviations to calculate statistical weights (Chung & Kennedy, 1991; Haran, 2004). These increases in standard deviation can also be used to detect transitions in the FRET time traces as we describe here.

Consider a data point at time t with a transition occurring between time t+2 and t+3 (Fig. 6). Using a predictor window of four data points, the standard deviation of both the forward and backward predictor windows can be calculated at each value of t. (Fig. 6 depicts these calculations for $t - 2$ to t+7.) In this example, the standard deviation of the forward predictor window at time t is at a local maximum. This maximum also occurs in the backward predictor window at time t+5 because both these windows contain the same range of data points. Accordingly, transitions can be detected by finding the midpoint between local maxima in the forward and backward predictor windows. To ensure only “real” transitions are kept, only the highest percentile local maxima are considered. By changing this percentile, the transitions can be scored for confidence. The most common source of false positives is bleaching and blinking events where either the donor or the acceptor fluorescence intensity is approximately zero. Regions of data previously identified as unanalyzable (i.e., bleaches and blinks) can be assigned a constant FRET not observed in the experiment, which eliminates their standard deviations and allows this transition detection method to function. Finally, a true change in FRET involves anticorrelated transitions in the donor and the acceptor signals (Haran, 2004). Including requirements that such anticorrelation be present above a threshold further aids confident identification of FRET transitions without falsely including bleaching and blinking events.

3.2.5 Alignment and Confirmation of Transitions in the FRET Time Traces—

Typically, the timing of each transition identified by both methods is in agreement; however, the two described methods occasionally produce slightly disparate results. In these instances, any transitions occurring within 0.3 s can be empirically aligned taking the weighted average of the time detected by each method. The weights used in this average can be determined using the confidence scores provided by each method.

Notably, both methods described here require user input to choose the appropriate thresholds. In the event that transitions are being missed (false negatives), the thresholds should be reduced. More often false transitions are identified. To test the significance of each transition, the FRET efficiency between each transition can be averaged, and the averages of adjacent FRET states can be subjected to a t-test. If two states are not statistically

significantly different from one another (p level 0.05), then the transition between the two states can be identified as a false positive and discarded.

3.2.6 User Interaction and FRET-TACKLE—In the analysis described so far, the user is only required for the initial input parameters, such as smoothing windows and transition detection thresholds; the rest of the analysis can be completed by a computer in batch. Upon completion of the batch analysis, the computationally determined transitions can be verified, and any remaining false positives in each molecule's FRET time trace can be discarded by hand. This process, though tedious, can be crucial to recognizing patterns or detecting systematic errors in the computational approach.

Once the transitions have been determined, FRET-TACKLE (FRET Transition Analysis Coupled with Kinetic Lifetime Evaluation) analysis can extract the pertinent mechanistic information from the compiled data (DeRocco et al., 2014; Sass et al., 2010). In this method, distinct molecular conformations are identified by their characteristic FRET and kinetic lifetime properties. This approach allows molecular states with the same FRET but distinct kinetics to be distinguished.

3.3 Modeling DNA MMR Complex Kinetics From smFRET Measurements

Analysis of the distribution of FRET efficiencies, the characteristic lifetimes, and the preferred transitions reveals conformational, kinetic, and pathway preference information for the protein:DNA complexes being studied, which can provide mechanistic insights. Sass et al. used smFRET measurements of *Taq* MutS induced bending at a GT mismatch to deduce that as many as six different conformations with different degrees of bending were sampled with complex kinetics (Sass et al., 2010). Some of these states had overlapping FRET levels, but were distinguishable by their lifetimes that varied by 20-fold and rates of intercoversion that differed by 2 orders of magnitude. From detailed modeling of the quantitative measurements of lifetimes of the states and their probabilities of making each possible transition, landmarks in the free energy landscape of the MutS interaction with a DNA mismatch could be deduced (DeRocco et al., 2014; Sass et al., 2010).

Using smFRET between MutS domain I donor and an acceptor 9 bases away from a DNA mismatch (Fig. 7A), Qiu et al. measured an ATP-dependent sequence of conformational changes that occurred during conversion of mismatch-bound MutS into a state of MutS that leaves the mismatch and slides along the DNA (Qiu et al., 2012). MutS bound to a mismatch in a configuration that yielded FRET ~0.7 (Fig. 7B and C). A precise kinetic pathway of states was observed in the subset of molecules that eventually converted to sliding clamps in the presence of ATP.

Before sliding away from the mismatch, a transition to an intermediate state near FRET 0.5 occurred (Fig. 7B and C). Kinetic analysis of the lifetimes of the FRET 0.7 and FRET 0.5 lifetimes indicated that these states were significantly different. Measurements of intraprotein FRET between donor and label on the two DNA binding domains of the MutS dimer confirmed this two-step process (Qiu et al., 2012). The histogram of the lifetimes of many occurrences of the 0.5 FRET state fit well to a single exponential decay with lifetime of 0.6 s, suggesting a single-step conformational change accounted for the change in FRET

level (Fig. 7D, lower). In contrast, the distribution of lifetimes of the 0.7 FRET state is clearly not a simple exponential decay (Fig. 7D, upper) (Qiu et al., 2015). The distribution rises at short times. It was well fit with a model of a two-step kinetic process that does not generate a conformational change leading to a distinct FRET value. Such a two-step process is characterized by lifetime distributions given by $k_1 * k_2 * (\exp(-k_1 * t) - \exp(-k_2 * t))/(k_2 - k_1)$, where k_1 and k_2 are the rates of the two distinct steps underling the process (Floyd, Harrison, & van Oijen, 2010; Yildiz et al., 2003). Fitting the experiments yields estimates of k_1 and k_2 as 1.1 ± 0.67 and 0.45 ± 0.02 s^{-1}. Preliminary experiments indicate that one of these rates is affected by ATP concentration and the other is not, suggesting that one of the steps involves ATP binding from solution. Addition of MutL, the next protein in the repair signaling cascade that interacts with mismatch activated MutS, did not change the FRET level of the first state, but did alter the kinetic behavior (Fig. 7E–G). Subsequent FRET states and kinetics were also modified. In particular, MutL prevented MutS from sliding away from the mismatch. Rather, MutS was observed to always dissociate directly from the mismatch under those experimental conditions (Qiu et al., 2015).

4. COMPLEMENTARITY BETWEEN SINGLE MOLECULE AND ENSEMBLE KINETICS: AN MMR CASE STUDY

Ensemble kinetic measurements performed on the millisecond time-scale of a single enzyme-catalyzed reaction cycle reveal the rates and order of multiple events, starting from substrate binding through transient conformational changes and catalysis and finally product release. For the MMR system, a combination of rapid-quench and stopped-flow experiments has outlined the kinetic mechanism employed by MutS as it uses ATPase activity to recognize and signal repair of mismatched bases in DNA. As with all ensemble methods, these rapid kinetic methods provide average measures of the population, which can obscure functionally significant distributions and dynamics of individual molecules, but they also yield detailed models of reaction pathways and enzyme mechanisms in solution. In this section, we use MutS to illustrate how single molecule and ensemble kinetic approaches complement each other to yield a richly textured view of the structure/dynamics–function relationships governing enzyme-catalyzed reactions.

4.1 DNA Binding and Bending by MutS

One key finding from the smFRET DNA binding measurements was that MutS forms a complex with mismatched DNA in bent conformation at a bimolecular rate constant of $1.3 \times 10^6\ M^{-1}\ s^{-1}$ (Sass et al., 2010). Stopped-flow experiments were also used to measure formation of the MutS:mismatched DNA complex, with different fluorescence-based assays monitoring MutS or DNA conformation during the reaction. MutS was mixed rapidly with DNA and the rates of signal change from fluorophore-labeled DNA or MutS were measured at increasing concentrations of the unlabeled reactant. Experiments with labeled DNA determined the following: (i) increase in fluorescence anisotropy of TAMRA-labeled DNA reported MutS:DNA complex formation, and linear dependence of the rate on MutS concentration yielded a binding rate constant of $6 \times 10^6\ M^{-1}\ s^{-1}$ (Jacobs-Palmer & Hingorani, 2007); (ii) increase in FRET between AF488 and AF594 fluorophores flanking the mismatch reported DNA bending in the MutS:DNA complex, and the initial linear rate

dependence on MutS concentration yielded a similar binding/DNA bending rate constant of $4 \times 10^6\ M^{-1}\ s^{-1}$ (Fig. 8A and B, pink). Experiments with MutS labeled with IAANS on the DNA binding domain I also yielded a similar binding/MutS conformational change rate constant of $7 \times 10^6\ M^{-1}\ s^{-1}$ (Fig. 8A and B, blue) (Sharma et al., 2013).

The agreement between single molecule and ensemble rates (measured by different reporter assays) validated the design and setup of smFRET experiments, indicating that there were no perturbations, for example, due to surface immobilization or fluorophore choice/position. In terms of the mismatch recognition mechanism, the smFRET data indicated that MutS binding to DNA occurs simultaneously with DNA bending. However, unlike single molecule, ensemble experiments allow measurements of fast rates and at high reactant concentrations, which ultimately revealed a different mechanism. As shown in Fig. 8B, the observed rates of DNA binding/bending and MutS conformational change show a linear dependence until ~3 μ*M* of MutS or DNA titrant, but at higher concentrations the rates saturate at 20–25 s^{-1}. This hyperbolic relationship is indicative of a two-step mechanism in which initial collision between MutS and DNA is followed by isomerization of both molecules that determines formation of the final high-affinity mismatch recognition complex (K_D ~ 10 n*M*) (Sharma et al., 2013). On the flip side, while the ensemble data resolved a sequential induced-fit mechanism of mismatch recognition, understanding the nature of the conformational changes in MutS and DNA required single-molecule analysis. smFRET experiments with labeled MutS showed that the DNA binding domains close in toward the mismatch to stabilize bent DNA in the MutS: DNA complex (Qiu et al., 2012), and smFRET experiments with labeled DNA showed that while MutS samples DNA conformations with varying degrees of bending, the complex with highly bent DNA is preferred kinetically and energetically (Sass et al., 2010).

4.2 ATPase-Coupled MutS Actions in MMR

Ensemble equilibrium and transient kinetic measurements of ATP binding, hydrolysis, and product release have revealed the MutS ATPase mechanism and enabled understanding of how it drives MutS actions before and after mismatch recognition (reviewed in Hingorani, 2016). Pre-steady-state rapid-quench experiments mixing MutS with ^{32}P-ATP measured the stoichiometry and the rate of ATP hydrolysis (^{32}P-ADP formation) and determined that off the mismatch, MutS binds and hydrolyzes only one ATP per dimer rapidly and then undergoes a slow rate-limiting step that defines the ~40-fold slower steady-state rate of the reaction (k_{cat}) (Fig. 8C, green). Pre-steady-state stopped-flow experiments mixing MutS with ATP and MDCC-PBP (fluorophore-labeled phosphate binding protein reporter) measured the stoichiometry and the rate of phosphate release after ATP hydrolysis. The data were identical to those from ^{32}P-ATP hydrolysis measurements, showing that free or mismatch-bound MutS releases the phosphate product rapidly (Antony & Hingorani, 2004). In contrast, stopped-flow experiments with Mant-ADP (fluorophore-labeled ADP analog) showed ADP dissociating slowly from free MutS, indicating that ADP product release limits the k_{cat} following ATP hydrolysis and phosphate release (Geng et al., 2012). Thus, off the mismatch, MutS remains predominantly bound to (at least one) ADP. Similar experiments performed with MutS:mismatched DNA complex showed stimulation of ADP release associated with rapid ATP binding; however, ATP hydrolysis was strongly suppressed by

~30–50-fold (Fig. 8C, red). Thus, on the mismatch, MutS remains predominantly bound to (two) ATP (Antony & Hingorani, 2004). To summarize, prior to mismatch recognition the ATPase mechanism favors a MutS population in which at least one ADP is stably bound per dimer, whereas after mismatch recognition the mechanism favors a MutS:mismatched DNA complex population in which two ATP are stably bound per dimer.

Analogous transient kinetic measurements of IAANS-labeled MutS show that the protein adopts one conformation rapidly at the rate of ATP binding (increasing fluorescence) and another at the rate of ATP hydrolysis (decreasing fluorescence; Fig. 8D, green). These results indicate binary switching of MutS between ATP-bound and ADP-bound forms with the latter persisting in steady state prior to mismatch recognition. When MutS binds a mismatch, it releases ADP and binds ATP rapidly (as determined from the experiments described above), but the conformational change after ATP binding is much slower and involves multiple steps (Fig. 8D, red, increasing fluorescence). Since ATP hydrolysis is suppressed in the MutS: mismatched DNA complex, these results indicate rate-determining conversion of ATP-bound MutS into a postmismatch recognition form that can signal repair. The nature of the nucleotide-coupled changes in MutS conformation and dynamics was again revealed by single-molecule analysis. smFRET between DNA binding domains I of the MutS dimer reported transitions between low (domains open) and high (domains closed) FRET for nucleotide-free and ADP-bound protein in the absence of mismatched DNA (Qiu et al., 2012). Thus the ADP-bound form of MutS, which is predominant prior to mismatch recognition, as described above, exhibits conformational dynamics that enable it to enclose DNA within the binding cavity (Fig. 1) and probe the duplex for mismatched bases. smFRET experiments also revealed that domains I lock into a closed conformation upon mismatch recognition, effectively stalling MutS at the site. As the MutS:mismatched DNA complex releases ADP and binds ATP, domains I transition slowly into a more open, stable conformation that enables ATP-bound MutS to interact with MutL and initiate repair, or disengage from the mismatch and slide away within a few seconds if MutL is not available (Fig. 7) (Qiu et al., 2012, 2015). Thus, ensemble measurements provided a framework to establish how MutS uses its ATPase reaction for mismatch recognition and initiation of repair. This information was not accessible by single-molecule methods due to a lack of reporter assays and inadequate temporal resolution. Single-molecule experiments provided complementary information on how ADP- and ATP-bound forms of MutS can recognize mismatches and license subsequent steps in the repair pathway, respectively. This information was not accessible by ensemble methods because of the inability to resolve conformational dynamics of individual MutS molecules on and off DNA.

5. CONCLUDING REMARKS

Here we have described smFRET methods to detect sequential conformational changes that occur when MMR proteins interact with a base–base mismatch or nucleotide insertion in DNA. By attaching donor and acceptor fluorophores on either DNA or protein, we developed assays sensitive to the degree of DNA bending, the relative positions of DNA binding domains in the MutS dimer, or the position of MutS on DNA relative to the mismatch. Automated edge detection in smFRET time traces enabled acquisition of sufficient quantitative data on conformational state transitions to statistically characterize the

kinetic behavior of these macromolecules. We also outlined a combined single molecule and ensemble kinetics approach that provided more comprehensive insights into MutS structure/dynamics and catalytic mechanism during the reaction. Future extensions of smFRET experiments to include additional MMR proteins, three and four fluorophore labels yielding multiple FRET signal combinations (DeRocco et al., 2010; Lee et al., 2010), and applications in live cells (Huang, Nagy, Koide, Rock, & Koide, 2009; Li & Xie, 2011; Reyes-Lamothe, Sherratt, & Leake, 2010; Sakon & Weninger, 2010; Uphoff, Reyes-Lamothe, Garza de Leon, Sherratt, & Kapanidis, 2013) are underway to complete understanding of the mechanisms of action of all proteins in this critical DNA repair pathway.

Acknowledgments

This work was supported by NIH Grants GM079480 and GM080294 (to D.A.E.), GM109832 (to D.A.E. and K.R.W.), and GM114743 (to M.M.H), and NSF Grant MCB-1022203 (to M.M.H.).

References

Antony E, Hingorani MM. Asymmetric ATP binding and hydrolysis activity of the *Thermus aquaticus* MutS dimer is key to modulation of its interactions with mismatched DNA. Biochemistry. 2004; 43(41):13115–13128. http://dx.doi.org/10.1021/bi049010t. [PubMed: 15476405]

Bignami M, Casorelli I, Karran P. Mismatch repair and response to DNA-damaging antitumour therapies. European Journal of Cancer. 2003; 39(15):2142–2149. [PubMed: 14522371]

Blanco M, Walter NG. Analysis of complex single-molecule FRET time trajectories. Methods in Enzymology. 2010; 472:153–178. http://dx.doi.org/10.1016/S0076-6879(10)72011-5. [PubMed: 20580964]

Brunger AT, Strop P, Vrljic M, Chu S, Weninger KR. Three-dimensional molecular modeling with single molecule FRET. Journal of Structural Biology. 2011; 173(3):497–505. http://dx.doi.org/10.1016/j.jsb.2010.09.004. [PubMed: 20837146]

Choi UB, Strop P, Vrljic M, Chu S, Brunger AT, Weninger KR. Single-molecule FRET-derived model of the synaptotagmin 1-SNARE fusion complex. Nature Structural & Molecular Biology. 2010; 17(3):318–324. http://dx.doi.org/10.1038/nsmb.1763.

Choi UB, Weninger KR, Bowen ME. Immobilization of proteins for single-molecule fluorescence resonance energy transfer measurements of conformation and dynamics. Methods in Molecular Biology. 2012; 896:3–20. http://dx.doi.org/10.1007/978-1-4614-3704-8_1. [PubMed: 22821514]

Chung SH, Kennedy RA. Forward-backward non-linear filtering technique for extracting small biological signals from noise. Journal of Neuroscience Methods. 1991; 40(1):71–86. http://dx.doi.org/10.1016/0165-0270(91)90118-J. [PubMed: 1795554]

DeRocco VC, Anderson T, Piehler J, Erie DA, Weninger K. Four-color single-molecule fluorescence with noncovalent dye labeling to monitor dynamic multimolecular complexes. Biotechniques. 2010; 49(5):807. [PubMed: 21091445]

DeRocco VC, Sass LE, Qiu R, Weninger KR, Erie DA. Dynamics of MutS-mismatched DNA complexes are predictive of their repair phenotypes. Biochemistry. 2014; 53(12):2043–2052. http://dx.doi.org/10.1021/bi401429b. [PubMed: 24588663]

Erie DA, Weninger KR. Single molecule studies of DNA mismatch repair. DNA Repair (Amst). 2014; 20:71–81. http://dx.doi.org/10.1016/j.dnarep.2014.03.007. [PubMed: 24746644]

Fedier A, Fink D. Mutations in DNA mismatch repair genes: Implications for DNA damage signaling and drug sensitivity (review). International Journal of Oncology. 2004; 24(4):1039–1047. [PubMed: 15010846]

Fishel R. Mismatch repair. Journal of Biological Chemistry. 2015; 290(44):26395–26403. http://dx.doi.org/10.1074/jbc.R115.660142. [PubMed: 26354434]

Floyd DL, Harrison SC, van Oijen AM. Analysis of kinetic intermediates in single-particle dwell-time distributions. Biophysical Journal. 2010; 99(2):360–366. http://dx.doi.org/10.1016/j.bpj.2010.04.049. [PubMed: 20643053]

Geng H, Sakato M, DeRocco V, Yamane K, Du C, Erie DA, … Hsieh P. Biochemical analysis of the human mismatch repair proteins hMutSalpha MSH2 (G674A)-MSH6 and MSH2-MSH6(T1219D). Journal of Biological Chemistry. 2012; 287(13):9777–9791. http://dx.doi.org/10.1074/jbc.M111.316919. [PubMed: 22277660]

Genschel J, Modrich P. Mechanism of 5′-directed excision in human mismatch repair. Molecular Cell. 2003; 12(5):1077–1086. [PubMed: 14636568]

Genschel J, Modrich P. Functions of MutLalpha, replication protein A (RPA), and HMGB1 in 5′-directed mismatch repair. Journal of Biological Chemistry. 2009; 284(32):21536–21544. http://dx.doi.org/10.1074/jbc.M109.021287. [PubMed: 19515846]

Greenfeld M, van de Meent JW, Pavlichin DS, Mabuchi H, Wiggins CH, Gonzalez RL Jr, Herschlag D. Single-molecule dataset (SMD): A generalized storage format for raw and processed single-molecule data. BMC Bioinformatics. 2015; 16:3. http://dx.doi.org/10.1186/s12859-014-0429-4. [PubMed: 25591752]

Groothuizen FS, Winkler I, Cristovao M, Fish A, Winterwerp HH, Reumer A, … Sixma TK. MutS/MutL crystal structure reveals that the MutS sliding clamp loads MutL onto DNA. eLife. 2015; 4:e06744. http://dx.doi.org/10.7554/eLife.06744. [PubMed: 26163658]

Ha T, Enderle T, Ogletree DF, Chemla DS, Selvin PR, Weiss S. Probing the interaction between two single molecules: Fluorescence resonance energy transfer between a single donor and a single acceptor. Proceedings of the National Academy of Sciences of the United States of America. 1996; 93(13):6264–6268. [PubMed: 8692803]

Haran G. Noise reduction in single-molecule fluorescence trajectories of folding proteins. Chemical Physics. 2004; 307(2–3):137–145. http://dx.doi.org/10.1016/j.chemphys.2004.05.017.

Heinen CD. Mismatch repair defects and Lynch syndrome: The role of the basic scientist in the battle against cancer. DNA Repair (Amst). 2016; 38:127–134. http://dx.doi.org/10.1016/j.dnarep.2015.11.025. [PubMed: 26710976]

Hingorani MM. Mismatch binding, ADP-ATP exchange and intramolecular signaling during mismatch repair. DNA Repair (Amst). 2016; 38:24–31. http://dx.doi.org/10.1016/j.dnarep.2015.11.017. [PubMed: 26704427]

Huang J, Nagy SS, Koide A, Rock RS, Koide S. A peptide Tag system for facile purification and single-molecule immobilization. Biochemistry. 2009; 48(50):11834–11836. http://dx.doi.org/10.1021/bi901756n. [PubMed: 19928925]

Iyer RR, Pluciennik A, Burdett V, Modrich PL. DNA mismatch repair: Functions and mechanisms. Chemical Reviews. 2006; 106(2):302–323. http://dx.doi.org/10.1021/cr0404794. [PubMed: 16464007]

Jacobs-Palmer E, Hingorani MM. The effects of nucleotides on MutS-DNA binding kinetics clarify the role of MutS ATPase activity in mismatch repair. Journal of Molecular Biology. 2007; 366(4):1087–1098. http://dx.doi.org/10.1016/j.jmb.2006.11.092. [PubMed: 17207499]

Kadyrov FA, Dzantiev L, Constantin N, Modrich P. Endonucleolytic function of MutLalpha in human mismatch repair. Cell. 2006; 126(2):297–308. http://dx.doi.org/10.1016/j.cell.2006.05.039. [PubMed: 16873062]

Kadyrov FA, Holmes SF, Arana ME, Lukianova OA, O'Donnell M, Kunkel TA, Modrich P. Saccharomyces cerevisiae MutLa is a mismatch repair endonuclease. Journal of Biological Chemistry. 2007; 282:37181–37190. [PubMed: 17951253]

Karran P, Offman J, Bignami M. Human mismatch repair, drug-induced DNA damage, and secondary cancer. Biochimie. 2003; 85(11):1149–1160. [PubMed: 14726020]

Kunkel TA, Erie DA. DNA mismatch repair. Annual Review of Biochemistry. 2005; 74:681–710.

Kunkel TA, Erie DA. Eukaryotic mismatch repair in relation to DNA replication. Annual Review of Genetics. 2015; 49:291–313. http://dx.doi.org/10.1146/annurev-genet-112414-054722.

Lakowicz, JR. Principles of fluorescence spectroscopy. 3. USA: Springer-Verlag; 2006.

Lamers MH, Perrakis A, Enzlin JH, Winterwerp HH, de Wind N, Sixma TK. The crystal structure of DNA mismatch repair protein MutS binding to a G x T mismatch. Nature. 2000; 407(6805):711–717. [PubMed: 11048711]

Lee J, Lee S, Ragunathan K, Joo C, Ha T, Hohng S. Single-molecule four-color FRET. Angewandte Chemie. 2010; 49(51):9922–9925. http://dx.doi.org/10.1002/anie.201005402. [PubMed: 21104966]

Li GW, Xie XS. Central dogma at the single-molecule level in living cells. Nature. 2011; 475(7356): 308–315. http://dx.doi.org/10.1038/nature10315. [PubMed: 21776076]

Liberti SE, Larrea AA, Kunkel TA. Exonuclease 1 preferentially repairs mismatches generated by DNA polymerase alpha. DNA Repair (Amst). 2013; 12(2):92–96. http://dx.doi.org/10.1016/j.dnarep.2012.11.001. [PubMed: 23245696]

McCann JJ, Choi UB, Zheng L, Weninger K, Bowen ME. Optimizing methods to recover absolute FRET efficiency from immobilized single molecules. Biophysical Journal. 2010; 99(3):961–970. http://dx.doi.org/10.1016/j.bpj.2010.04.063. [PubMed: 20682275]

McKinney SA, Joo C, Ha T. Analysis of single-molecule FRET trajectories using hidden Markov modeling. Biophysical Journal. 2006; 91(5):1941–1951. http://dx.doi.org/10.1529/biophysj.106.082487. [PubMed: 16766620]

Modrich P, Lahue R. Mismatch repair in replication fidelity, genetic recombination, and cancer biology. Annual Review of Biochemistry. 1996; 65:101–133.

Morita R, Nakane S, Shimada A, Inoue M, Iino H, Wakamatsu T, … Kuramitsu S. Molecular mechanisms of the whole DNA repair system: A comparison of bacterial and eukaryotic systems. Journal of Nucleic Acids. 2010; 2010:179594. http://dx.doi.org/10.4061/2010/179594. [PubMed: 20981145]

Natrajan G, Lamers MH, Enzlin JH, Winterwerp HH, Perrakis A, Sixma TK. Structures of *Escherichia coli* DNA mismatch repair enzyme MutS in complex with different mismatches: A common recognition mode for diverse substrates. Nucleic Acids Research. 2003; 31(16):4814–4821. [PubMed: 12907723]

Nick McElhinny SA, Kissling GE, Kunkel TA. Differential correction of lagging-strand replication errors made by DNA polymerases {alpha} and {delta}. Proceedings of the National Academy of Sciences of the United States of America. 2010; 107(49):21070–21075. http://dx.doi.org/10.1073/pnas.1013048107. [PubMed: 21041657]

Obmolova G, Ban C, Hsieh P, Yang W. Crystal structures of mismatch repair protein MutS and its complex with a substrate DNA. Nature. 2000; 407(6805):703–710. http://dx.doi.org/10.1038/35037509. [PubMed: 11048710]

Pavlov YI, Mian IM, Kunkel TA. Evidence for preferential mismatch repair of lagging strand DNA replication errors in yeast. Current Biology. 2003; 13(9):744–748. [PubMed: 12725731]

Peltomaki P. Update on Lynch syndrome genomics. Familial Cancer. 2016; 15:385–393. http://dx.doi.org/10.1007/s10689-016-9882-8. [PubMed: 26873718]

Pluciennik A, Burdett V, Lukianova O, O'Donnell M, Modrich P. Involvement of the beta clamp in methyl-directed mismatch repair in vitro. The Journal of Biological Chemistry. 2009; 284(47): 32782–32791. http://dx.doi.org/10.1074/jbc.M109.054528. [PubMed: 19783657]

Qiu R, DeRocco VC, Harris C, Sharma A, Hingorani MM, Erie DA, Weninger KR. Large conformational changes in MutS during DNA scanning, mismatch recognition and repair signalling. The EMBO Journal. 2012; 31(11):2528–2540. http://dx.doi.org/10.1038/emboj.2012.95. [PubMed: 22505031]

Qiu R, Sakato M, Sacho EJ, Wilkins H, Zhang X, Modrich P, … Weninger KR. MutL traps MutS at a DNA mismatch. Proceedings of the National Academy of Sciences of the United States of America. 2015; 112(35):10914–10919. http://dx.doi.org/10.1073/pnas.1505655112. [PubMed: 26283381]

Reyes-Lamothe R, Sherratt DJ, Leake MC. Stoichiometry and architecture of active DNA replication machinery in *Escherichia coli*. Science. 2010; 328(5977):498–501. http://dx.doi.org/10.1126/science.1185757. [PubMed: 20413500]

Sakon JJ, Weninger KR. Detecting the conformation of individual proteins in live cells. Nature Methods. 2010; 7(3):203–205. http://dx.doi.org/10.1038/nmeth.1421. [PubMed: 20118931]

Sass LE, Lanyi C, Weninger K, Erie DA. Single-molecule FRET TACKLE reveals highly dynamic mismatched DNA-MutS complexes. Biochemistry. 2010; 49(14):3174–3190. [PubMed: 20180598]

Schofield MJ, Nayak S, Scott TH, Du C, Hsieh P. Interaction of *Escherichia coli* MutS and MutL at a DNA mismatch. Journal of Biological Chemistry. 2001; 276(30):28291–28299. http://dx.doi.org/10.1074/jbc.M103148200. [PubMed: 11371566]

Sharma A, Doucette C, Biro FN, Hingorani MM. Slow conformational changes in MutS and DNA direct ordered transitions between mismatch search, recognition and signaling of DNA repair. Journal of Molecular Biology. 2013; 425(22):4192–4205. http://dx.doi.org/10.1016/j.jmb.2013.08.011. [PubMed: 23973435]

Shuang B, Cooper D, Taylor JN, Kisley L, Chen J, Wang W, … Landes CF. Fast step transition and state identification (STaSI) for discrete single-molecule data analysis. Journal of Physical Chemistry Letters. 2014; 5(18):3157–3161. http://dx.doi.org/10.1021/jz501435p. [PubMed: 25247055]

Stryer L, Haugland RP. Energy transfer: A spectroscopic ruler. Proceedings of the National Academy of Sciences of the United States of America. 1967; 58(2):719–726. [PubMed: 5233469]

Uphoff S, Reyes-Lamothe R, Garza de Leon F, Sherratt DJ, Kapanidis AN. Single-molecule DNA repair in live bacteria. Proceedings of the National Academy of Sciences of the United States of America. 2013; 110(20):8063–8068. http://dx.doi.org/10.1073/pnas.1301804110. [PubMed: 23630273]

van de Meent JW, Bronson JE, Wiggins CH, Gonzalez RL Jr. Empirical Bayes methods enable advanced population-level analyses of single-molecule FRET experiments. Biophysical Journal. 2014; 106(6):1327–1337. http://dx.doi.org/10.1016/j.bpj.2013.12.055. [PubMed: 24655508]

Wang H, Yang Y, Schofield MJ, Du C, Fridman Y, Lee SD, … Erie DA. DNA bending and unbending by MutS govern mismatch recognition and specificity. Proceedings of the National Academy of Sciences of the United States of America. 2003; 100(25):14822–14827. http://dx.doi.org/10.1073/pnas.2433654100. [PubMed: 14634210]

Warren JJ, Pohlhaus TJ, Changela A, Iyer RR, Modrich PL, Beese LS. Structure of the human MutSalpha DNA lesion recognition complex. Molecular Cell. 2007; 26(4):579–592. [PubMed: 17531815]

Yildiz A, Forkey JN, McKinney SA, Ha T, Goldman YE, Selvin PR. Myosin V walks hand-over-hand: Single fluorophore imaging with 1.5-nm localization. Science. 2003; 300(5628):2061–2065. http://dx.doi.org/10.1126/science.1084398. [PubMed: 12791999]

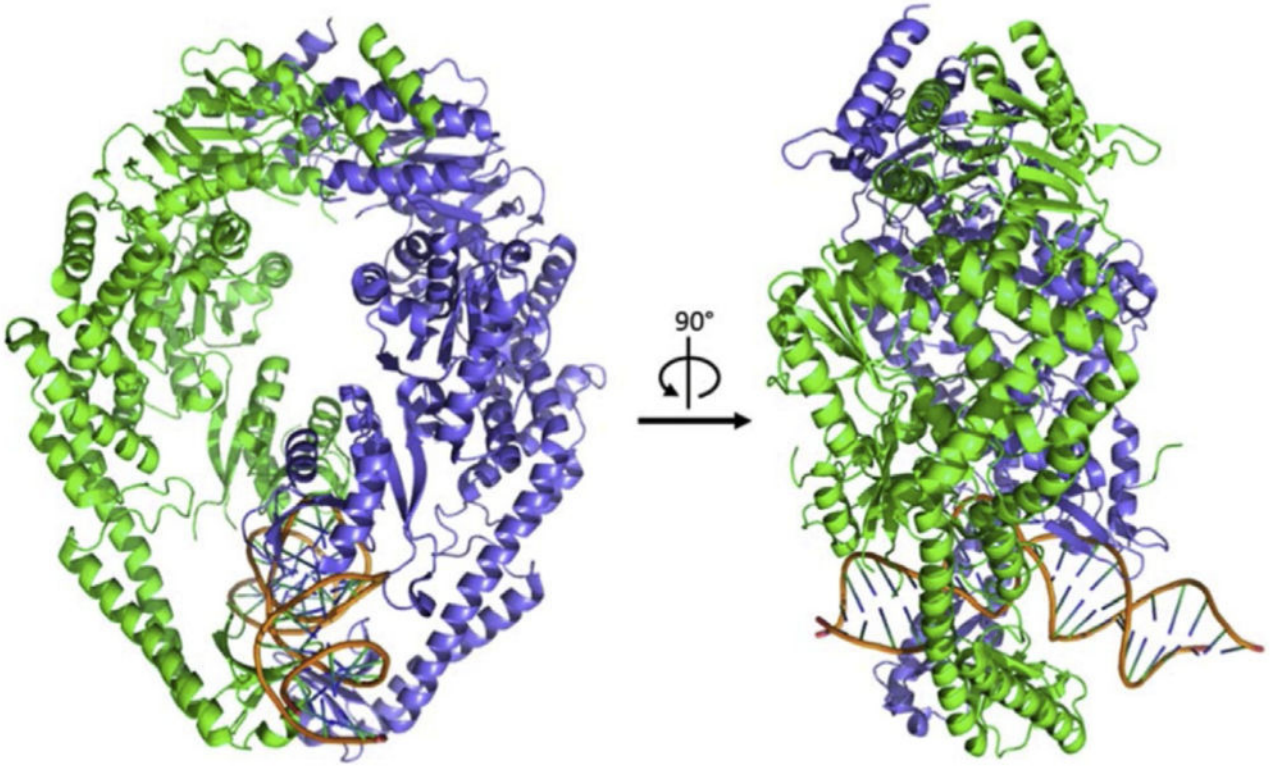

Fig. 1.

Front view (*left*) and *side* view (*right*) of *Taq* MutS in complex with DNA containing a single thymine insertion (PDB ID: 1EWQ). The two subunits of the homodimer are colored *blue* and *green*, and the DNA is shown in *orange* (Obmolova et al., 2000).

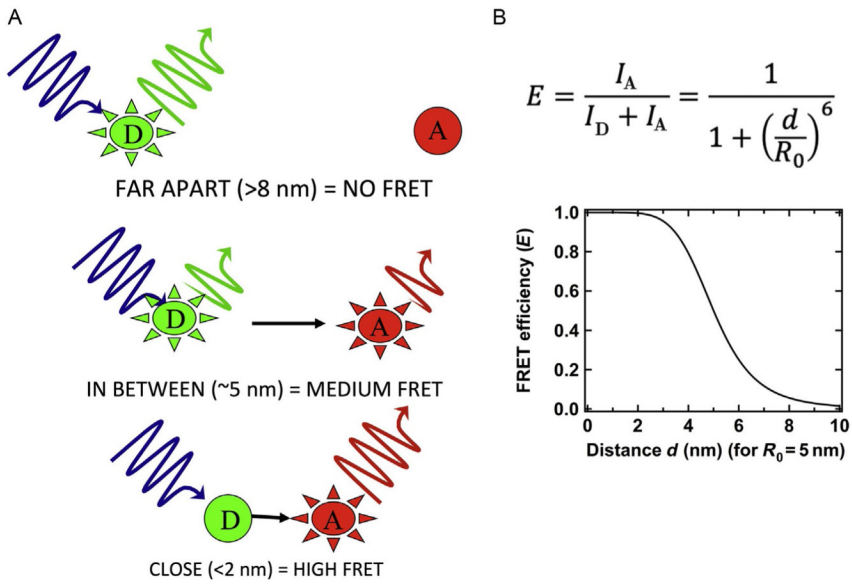

Fig. 2.

Overview of the concept of FRET. (A) Schematic illustrating FRET exchange between the donor fluorophore (D, *green*) and the acceptor fluorophore (A, *red*). Donor fluorescence is excited by the external light source (*blue*), and as the distance between D and A decreases, emission from D decreases and emission from A increases. (B) The relation between FRET efficiency (E) and the separation of the fluorophores d is scaled by the R_0 parameter. Here R_0 = 5 nm is used.

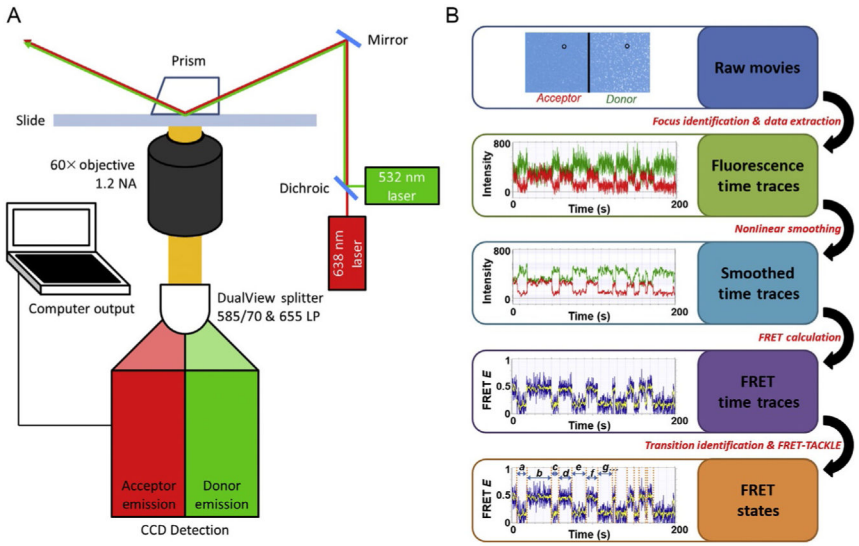

Fig. 3.

Optical setup and data analysis pipeline. (A) An example of the total internal reflection fluorescence microscope. (B) A schematic of the data analysis pipeline. The specific trace is from experiments measuring DNA bending by MutS at a T-bulge mismatch by the method diagramed in Fig. 4A.

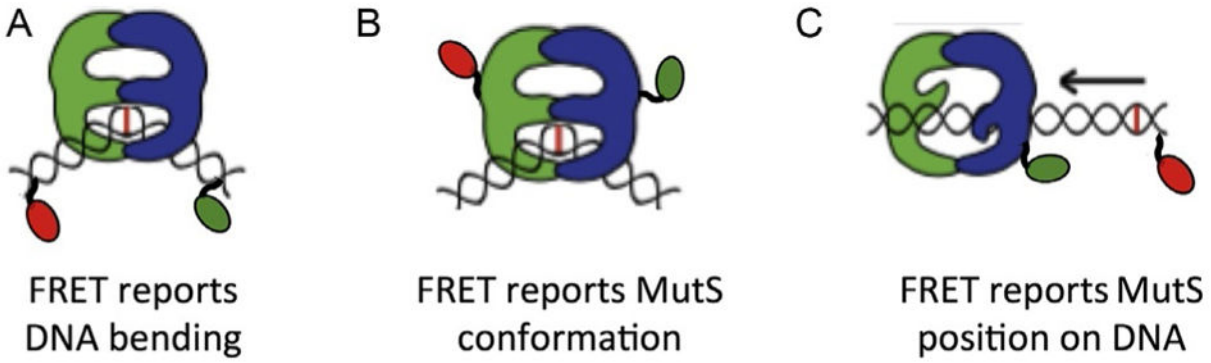

Fig. 4.

Schematic of the types of FRET signals utilized in DNA MMR assays. FRET can report (A) DNA bending if both donor and acceptor are on the DNA flanking the mismatch, (B) MutS conformation if both donor and acceptor are on the protein, and (C) relative distance between a domain of MutS and a site on DNA if acceptor is on the DNA and donor is on MutS.

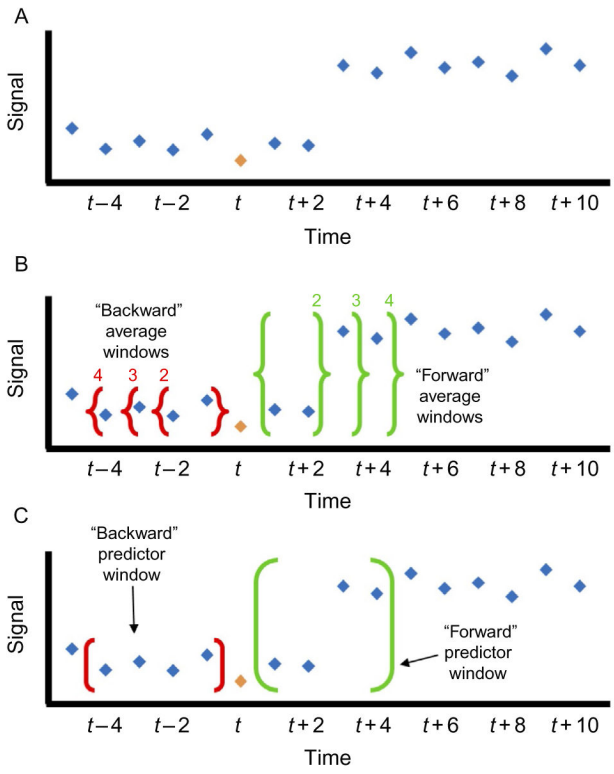

Fig. 5.

Chung–Kennedy smoothing algorithm. (A) An example of data containing a transition between $t+2$ and $t+3$. (B) A schematic depicting three sizes of "forward" (*green*) and "backward" (*red*) average windows. (C) A schematic depicting four-point "forward" (*green*) and "backward" predictor windows.

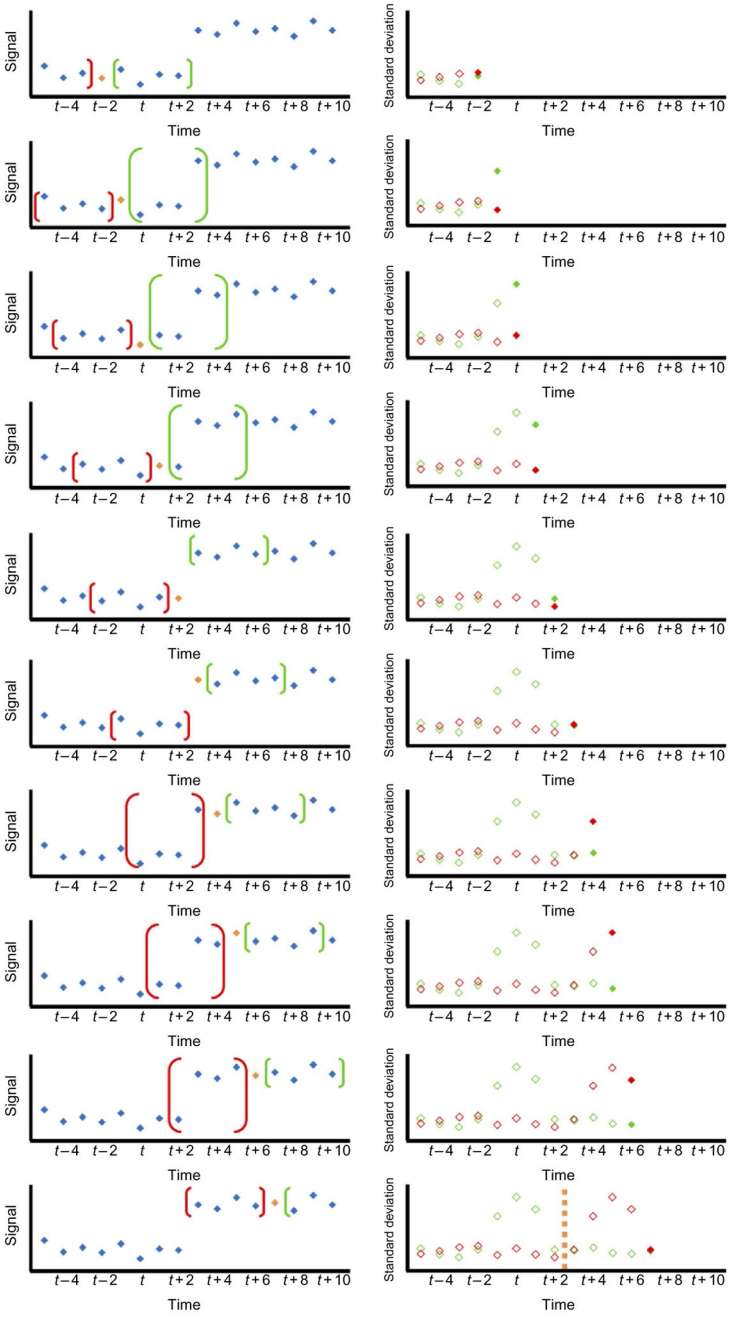

Fig. 6.

A novel transition detection method based on the Chung–Kennedy filter. “Forward” and “backward” predictor windows (*left column*, *green* and *red brackets*, respectively) are shown for successive time points (*blue diamonds*). Standard deviations for the depicted predictor windows (*right column*) reveal two identical peaks. Note that the midpoint between these peaks (between $t+2$ and $t+3$) identifies the time of the transition in the data.

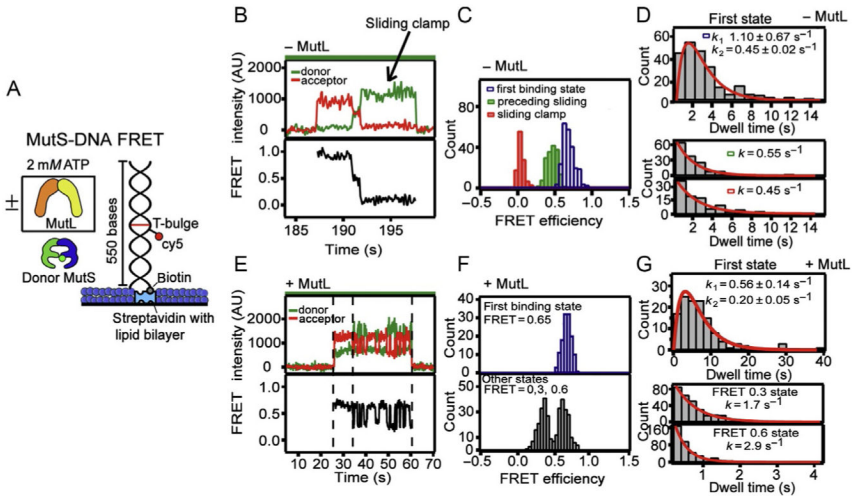

Fig. 7.

smFRET measurements of the kinetics of MutS mismatch recognition and subsequent conformational changes. (A) Experimental scheme: 2 m*M* ATP, 10 n*M* Alexa555-MutS, Cy5-T-bulge DNA, and 200 n*M* unlabeled MutL (when present). Example time traces of donor and acceptor emission and calculated FRET in the absence (B) and presence (E) of MutL for events with transitions. FRET histograms for binding events with exactly one donor and one acceptor and with FRET transitions reveal three states in the absence of MutL (C) with dwell time distributions fit (*red line*) by a two-step model for the first state (D, *top panel*) and a one-step model for the middle state and last state (D, *middle and lower panels*). In the presence of MutL, FRET histograms for the first state (F, *top panel*) reveal a narrow peak, but the dwell time distributions (G, *top panel*) still require a fit (*red line*) with two steps. Histograms of the subsequent FRET states show two nonzero peaks (F, *lower panel*), and the dwell time distributions are fit well (*red line*) with a one-step model (G, *middle* and *lower panels*). *Numbers within panels* report rates obtained from the fits. *Adapted from Qiu, R., Sakato, M., Sacho, E. J., Wilkins, H., Zhang, X., Modrich, P., … Weninger, K. R. (2015). MutL traps MutS at a DNA mismatch.* Proceedings of the National Academy of Sciences of the United States of America, 112*(35), 10914–10919. doi:10.1073/pnas.1505655112.*

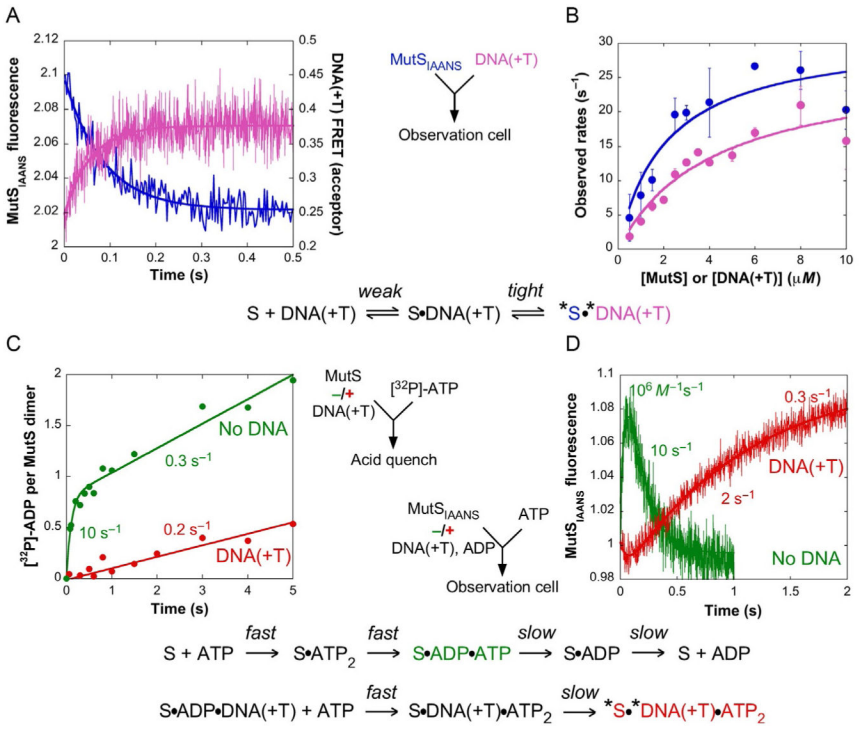

Fig. 8.

Stopped-flow studies of MMR proteins. (A) In stopped-flow experiments, IAANS fluorescence quenching reports MutS domain I movement on DNA binding (0.1 μ*M* $MutS_{IAANS}$ mixed with 3 μ*M* DNA(+T); *blue trace*), and increasing FRET between AF488 and AF594 flanking the T-bulge reports DNA bending on MutS binding (0.03 μ*M* $DNA(+T)_{AF488–AF594}$ mixed with 3 μ*M* MutS; *pink trace*). (B) The rates of these conformational changes increase hyperbolically with titrant concentration to a maximum of ~25 s^{-1} and fit to a two-step binding model with initial rapid collision forming a weak complex followed by intramolecular conformational changes to form a tight complex (K_D ~ 10 n*M*). (C) Pre-steady-state rapid-quench experiments with MutS reveal a burst of ^{32}P-ADP formation at 10 s^{-1} (40°C) followed by slow steady state k_{cat} = 0.3 s^{-1} (*green trace*). The burst amplitude indicates rapid hydrolysis of one ATP per MutS dimer. Pre-incubation of MutS with T-bulge DNA results in the inhibition of the burst and a slow ATPase rate of 0.2 s^{-1} (*red trace*). (D) Stopped-flow traces of $MutS_{IAANS}$ mixed with ATP show that domains I rearrange concurrently with ATP binding (signal increase) and switch right back with ATP hydrolysis (signal decrease), whereas one ADP-bound $MutS_{IAANS}$–DNA(+T) complex shows a lag (likely reflecting ADP release) followed by slow change in MutS conformation (signal increase) to a stable ATP-bound MMR ready complex. *Adapted from* Hingorani, M. M. (2016). *Mismatch binding, ADP-ATP exchange and intramolecular signaling during mismatch repair.* DNA Repair (Amst), 38*, 24–31. doi:10.1016/j.dnarep.2015.11.017.*